DOI: 10.1002/ ((please add manuscript number))

Article type: Full paper

Temperature-Dependent Aggregation Donor Polymers Enables Highly Efficient Sequentially Processed Organic Photovoltaics without the Need of Orthogonal Solvents

Lingeswaran Arunagiri, Guangye Zhang, Huawei Hu, Huatong Yao, Kai Zhang, Yunke Li, Philip C. Y. Chow, Harald Ade, and He Yan**

L. Arunagiri, Dr. G. Zhang, H. Yao, Dr. K. Zhang, Dr. Y. Li, Dr. P. C. Y. Chow, Prof. H. Yan
The Hong Kong University of Science and Technology-Shenzhen Research Institute, No. 9 Yuexing 1st RD, Hi-tech Park, Nanshan, Shenzhen 518057, P. R. China
L. Arunagiri, Dr. G. Zhang, H. Yao, Dr. K. Zhang, Dr. Y. Li, Dr. P. C. Y. Chow, Prof. H. Yan
Department of Chemistry and Hong Kong Branch of Chinese National Engineering Research Center for Tissue Restoration and Reconstruction, Hong Kong University of Science and Technology, Clear Water Bay, Kowloon, Hong Kong
E-mail: gyzhang@ust.hk; hyan@ust.hk
Dr. H. Hu, Prof. H. Ade
Department of Physics and ORganic and Carbon Electronics Labs (ORaCEL), North Carolina State University, Raleigh, North Carolina 27695, USA.

Keywords: organic photovoltaics, sequential processing method, bulk heterojunction, non-orthogonal solvents, temperature-dependent aggregation

Abstract

The conventional method to prepare bulk-heterojunction (BHJ) organic photovoltaics (OPVs) is a one-step method from the blend solution of donor and acceptor materials, known as blend-casting (BC). Recently, an alternative method was demonstrated to achieve high efficiencies (13%) comparable to state-of-the-art BC devices. This two-step-coating method, known as "sequential processing (SqP)," involves sequential deposition of the donor and then the acceptor from two orthogonal solvents. However, the requirement of orthogonal solvents

to process the donor and acceptor constrain the choice of materials and processing solvents. In this paper, we report an improved version of SqP method without the need of using orthogonal solvents. Our success is based on donor polymers with strong temperature-dependent aggregation (TDA) property whose solution can be processed at high temperature, but the resulting film becomes completely insoluble at room temperature, which allows for the processing of overlying acceptors from a wide range of non-orthogonal solvents. With this approach, we demonstrate efficient SqP OPV based on a range of donor/acceptor materials, processing solvents, and, in every single case, SqP OPV can outperform their BC counterparts. Our results broaden the solvent choices and open a much larger window to optimize the processing parameters of SqP method.

1. Introduction

In recent years, due to the impressive development of non-fullerene acceptors (NFAs),[1-14] power conversion efficiency (PCE) of over 14% have been achieved for single/multi-junction bulk-heterojunction (BHJ) architecture organic photovoltaics (OPVs).[15-19] In general, BHJ morphology is prepared using a one-step method from the blend solution of donor and acceptor materials, which is denoted as the blend-casting (BC) method herein. The formation of nano-scale BHJ morphology is quite complicated which requires desirable donor/acceptor (D/A) interface for efficient exciton dissociation and a bicontinuous interpenetrating network for better charge transportation for OPV devices to perform efficiently.[20-22] Hence, effective control of BHJ morphology is the key to develop efficient and scalable OPV.[21,23-29]

Recently, a promising alternative method, which is known as "sequential processing (SqP)," was developed.[30-39] In this method, the donor and acceptor layers are cast sequentially using two different solutions. Unlike BC, which relies on spontaneous de-mixing of D/A molecules, SqP depends on the degree of polymer swelling and the mass action

driving force of acceptors (related to thermodynamics) to intercalate into the amorphous regions of the polymer film.[34] Besides achieving higher efficiency, better scaling-up, thermal- and photostability have also been reported.[37,39] However, the main problem of SqP method is that the donor and the acceptor materials need to be processed from two different solvents which are orthogonal to each other. Otherwise, it is entirely possible for the underlying polymer film to get destroyed wholly or partially after spin casting the acceptor on top of it. Therefore, most of the reports are based on carefully choosing an orthogonal/quasi-orthogonal solvent either by using low boiling point solvent(s) (e.g., CF, THF, DCM) or including a small amount of high boiling point solvent (typically used as a co-solvent) for better interdiffusion of acceptor molecules.[36,38-39] Despite the high-performance, limited choices of acceptor's solvent could seriously hinder industrial production. For instance, to meet the orthogonal solvent requirement, one might lose the option of using high boiling point solvents (sometimes necessary for blade or slot-die coating) or using an eco-friendly solvent for green production.

In this work, we demonstrate efficient SqP OPV devices (PCE up to 11.8%) without the need of any orthogonal solvents. We use series of conjugated polymers with TDA property, which allows the polymer to disaggregate at higher temperatures (e.g., 100 °C) and aggregates as the solution cools down to room temperature: this helps to control the polymer crystallization with desirable domain size.[40-42] We took benefit of this distinctive property to process all our polymers from hot solutions using high boiling point solvents; by doing so, we can process our overlying acceptor layer using a wide range of solvents without the underlying polymer layer being washed away or extensively destroyed. The broadened choices of solvent are demonstrated on both fullerene and non-fullerene systems. Our processing conditions create a vertical distribution D/A morphology which allows us to use

conventional and inverted device configurations achieving comparable performance in both cases. To our knowledge, this is the first time, in SqP OPV using NFAs, that an acceptor has been processed using as many as five different solvents giving almost similar performance in each case. Also, as-cast samples (no post-thermal treatment) can perform as good as thermally annealed ones with only a slight difference in the performance proving that the acceptor can diffuse-in and blend well with the donor polymer even without any post-treatment.

We use dynamic secondary-ion mass spectroscopy (DSIMS) measurement to analyze the vertical phase distribution of the entire active layer film by tracing the elements of individual material. Along with this, we assessed other morphological characterization techniques including Grazing-Incidence Wide-Angle X-ray Scattering (GIWAXS) and Resonant Soft X-ray Scattering (RSoXS). To better understand the device performance between SqP and BC OPVs, we additionally analyzed the charge recombination mechanism in the devices using light intensity studies. These results demonstrate that using TDA materials which has no constraint in the usage of solvents; it is feasible to achieve and control the desired active layer morphology with more-ideal domain size and better crystallinity for fabricating efficient large-area modules with the likelihood of commercialization in the future.

2. Results and Discussion

2.1. OPV Device Materials and Performance

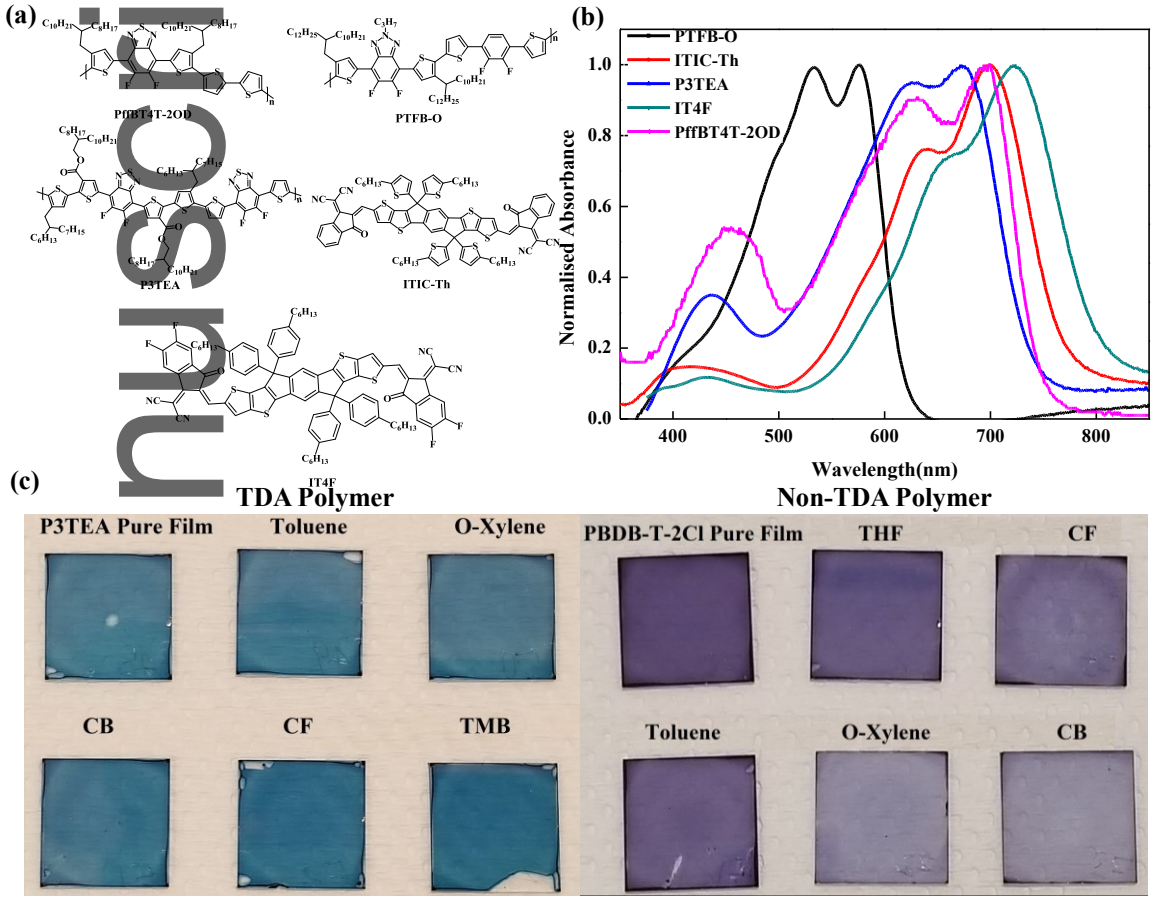

Figure 1. a) Chemical structures, b) UV-Vis absorption spectra of the donor and acceptor materials, and c) Comparison of TDA (P3TEA) versus non-TDA (PBDB-T-2Cl) polymers based pure films after spin-coating several solvents on top of it.

Our group previously published series of donor polymers, such as PffBT4T-2OD[43], PTFB-O[44], and P3TEA[1], which are known to exhibit the TDA property. Fullerene ($PC_{71}BM$) and non-fullerene acceptors (ITIC-Th[45], and IT4F[46]) are used to make binary SqP and BC devices. **Figure 1**a,b shows the chemical structures and UV-Vis absorption spectra of the donor and acceptor materials used in this report (**Figure S1** energy level diagram). OPV

devices were fabricated in two different device configurations: conventional and inverted. For conventional structure, we use indium tin oxide (ITO)/PEDOT:PSS/active layer/PFN-Br/Ag and for inverted structure, we use ITO/ZnO/active layer/MoO_3 + PEDOT:PSS mix (solution processable) or MoO_3 (thermally evaporated)/Ag. These device configurations are used to make both SqP and BC devices.

Figure S2 illustrates the SqP active layer morphology formation by a spin-coating technique. First, the TDA donor polymer is spun from a hot solution which is maintained at 100 °C (including the substrate), and by the time it cools down to room temperature, acceptor from a different solution is spun above the donor polymer film. Then, an optional post thermal treatment (depending on the material combination) creates a BHJ-like morphology. Generally, the degree of polymer swelling can be determined by the solvents which are used to process the top acceptor layers,[32-33] and other reasons including, but not limited to, the chemical nature of the acceptor, the crystallinity of the polymer,[33] the surface energy differences between polymer and acceptor,[47] determines how well the acceptor can drive itself into the bottom of the polymer film. Hence, the solvent of the acceptor is chosen in such a way that it helps the polymer to swell well without dissolving it. Since TDA materials have low solubility at room temperature,[40] we took advantage of this feature to process the acceptors even using high boiling point solvents like o-Xylene or chlorobenzene (CB). **Figure 1**c shows the comparison of pure donor films before and after spin-coating various solvents (UV-Vis absorption comparison in **Figure S4** and thickness measurements in **Table S4**), and it confirms that even the high boiling point solvent like TMB does not destroy the neat TDA polymer film, which is a common problem for non-TDA materials that do not exhibit this property. When solvents are spun on non-TDA polymer (e.g., PBDB-T-2Cl), it can be seen clearly that the polymer film is wholly/partially washed away. Those solvents

that extensively dissolve the underlayer film make it impossible to achieve an efficient device, which severely limits the choice of solvents for the acceptors.

We begin our exploration with fullerene-based devices. To examine the effectiveness of TDA polymer on the solvent choice for fullerenes, we used the SqP method to fabricate PffBT4T-2OD/$PC_{71}BM$ devices in the inverted device structure, where different solvents/solvent combinations were employed to process the fullerene. Thanks to the TDA property of PffBT4T-2OD, all solvents we compared (CB, ODCB, CF, and other solvent combinations) offered similar OPV performance (**Table S1**). We found that after thermal annealing, all solvents were able to achieve near-uniform vertical phase segregation throughout the active layer (**Figure S3**).

Motivated by these results, we fabricated a series of non-fullerene OPV devices using high-performance small molecular acceptors and TDA donor materials. For PTFB-O based SqP devices, the donor material is dissolved in CB, and the acceptor material (ITIC-Th) is dissolved either in tetrahydrofuran (THF) or chloroform (CF) or toluene. After spin-coating both donor and acceptor films, thermal annealing at 100 °C for 10 minutes was carried out. Also, for comparison, we fabricated PTFB-O based BC devices where the active layer was dissolved in CB with the weight ratio of 1:1.5 (PTFB-O:ITIC-Th). The same preparation conditions have been used to fabricate both conventional as well as inverted structures. For SqP devices, the best performance was achieved when the total thickness of the active layer film is ~100 nm. To have a fair comparison of the device performance, we kept the thickness of BC active layer film fixed to ~100 nm (verified by both ellipsometer, and surface profiler), which is also the thickness for best BC device performance. Therefore, our comparison is based on devices for SqP and BC that show the best device performance and, in the meantime, have the same thickness. Since the performance is highly dependent on D:A

composition, we matched the D:A composition of SqP and BC active layer film using UV-Visible absorption spectrum as shown in **Figure 2**b.

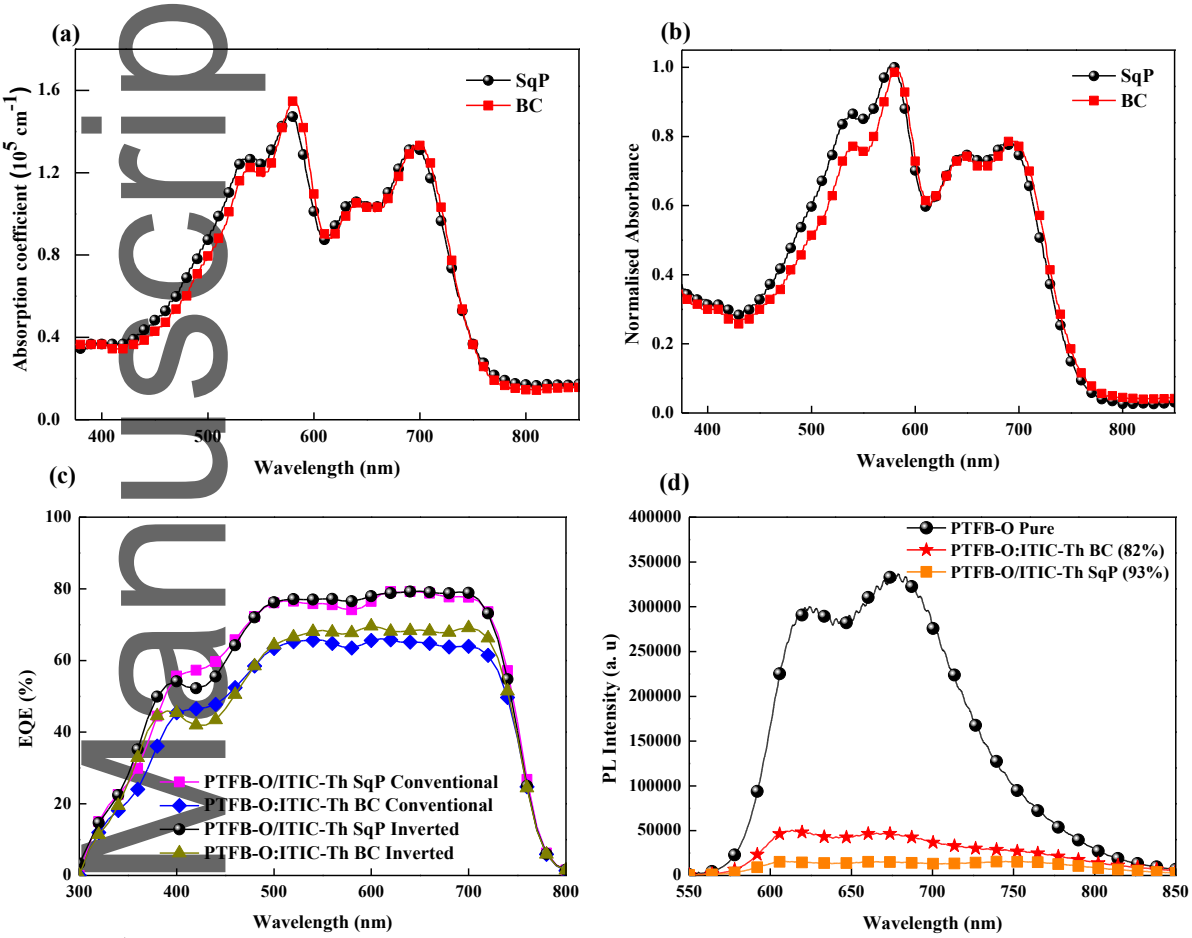

Figure 2. a) Absorption coefficient, and b) UV-Vis absorption spectra of SqP and BC films with the same thickness, c) EQE spectra of SqP and BC OPV devices for both conventional and inverted device configurations, and d) PL spectra of SqP and BC films where the values in the bracket are the PL quenching rate.

Table 1 shows the photovoltaic performances of PTFB-O based OPV devices. First and foremost, all three solvents we compared (THF, CF, and toluene) provided the SqP devices with comparable solar cell performances, which confirms the effectiveness of our strategy and highlights the role of the TDA polymer in broadening the solvent choice for the

acceptor. For conventional SqP devices, the best PCE is found to be 11.8% which is approximately 15% higher than that of the BC counterpart with similar thickness and composition. The superior performance of SqP devices comes mainly from its J_{SC}, which is, on average, ~2 mA/cm^2 higher than that of BC devices and the rationale will be discussed in later sections. The most exciting aspect of SqP method is that its inverted structure can outperform BC conventional/inverted devices as well, which is elucidated in detail in later sections. As mentioned previously, the SqP's active layer processing condition is similar for both conventional and inverted device configurations. In this scenario, the charge transportation is more favorable for conventional device configuration as PTFB-O is spun first followed by NFAs.

Simple characterizations like external quantum efficiency (EQE) and photoluminescence (PL) measurements were carried out to interpret the differences in performance between SqP and BC method. From EQE spectrum (**Figure 2**c), SqP devices possess higher EQE value of close to 80% between 500 to 700 nm, whereas BC devices show lower EQE value (65-70%) over the same range. Also, to better correlate the difference in J_{SC} between SqP and BC devices, PL quenching measurement was carried out as shown in **Figure 2**d. Generally, PL quenching reflects the charge transfer efficiency between donor polymer and acceptor making the device work efficiently.[48] Neat PTFB-O show strong PL between the range of 550-800 nm, and this is quenched by the addition of ITIC-Th which indicates efficient exciton dissociation.[49] The quenching efficiency of the SqP film (93%) is superior to their BC analog (82%), thus indicating more efficient exciton dissociation. As we formulate below, the relatively low PL quenching in the BC blend is largely due to the larger domain size.

Table 1. Photovoltaic performances of PTFB-O based OPV devices

Active Layer Combinations	V_{OC} [V]	J_{SC} [mA/cm^2]	FF	PCE[a] [%]	α[b]	n_{ideal}[c]
SqP Conventional PTFB-O/ITIC-Th (THF)	0.910 (0.913±0.004)	17.5 (17±0.2)	0.74 (0.74±0.01)	11.8 (11.4±0.2)	0.99	1.16±0.01
SqP Conventional PTFB-O/ITIC-Th (CF)	0.904 (0.905±0.003)	17.2 (17.1±0.1)	0.75 (0.74±0.01)	11.6 (11.4±0.1)	0.97	1.09±0.01
SqP Conventional PTFB-O/ITIC-Th (Toluene)	0.922 (0.919±0.002)	16.8 (16.5±0.2)	0.76 (0.75±0.01)	11.7 (11.4±0.2)	0.97	1.12±0.02
SqP Conventional PTFB-O/ITIC-Th (As-cast)	0.924 (0.923±0.004)	16.3 (16.4±0.2)	0.75 (0.73±0.01)	11.4 (11.1±0.2)	0.97	1.15±0.01
SqP Inverted PTFB-O/ITIC-Th (THF)	0.868 (0.869±0.007)	17.9 (17.8±0.2)	0.70 (0.69±0.01)	11.0 (10.7±0.1)	0.99	1.15±0.05
BC Conventional PTFB-O:ITIC-Th	0.926 (0.926±0.006)	14.9 (14.9±0.2)	0.75 (0.75±0.01)	10.4 (10.3±0.1)	0.97	1.22±0.04
BC Inverted PTFB-O:ITIC-Th	0.867 (0.868±0.003)	15.6 (15.5±0.1)	0.70 (0.69±0.01)	9.5 (9.3±0.2)	0.96	1.51

[a)]The standard deviations are based on measurements of over at least ten independent devices; [b)]The slope from a linear fit of J_{SC} versus log$I$; [c)] Ideality factors (n_{ideal}) obtained from analyzing V_{OC}–light intensity data.

2.2. Morphological Characterization and its Association to OPV Device Performances

Our results show that regardless of device configurations, the SqP devices can outclass BC devices and it intrigued us why the better performance can be achieved for both the device configurations? To answer this question and explain the higher PL quenching efficiency of the SqP film, morphological characterizations such as GIWAXS and R-SoXS measurements were carried out. Using GIWAXS, molecular packing and ordering of pure PTFB-O, PTFB-O/ITIC-Th SqP, and PTFB-O:ITIC-Th BC films are extracted and compared. Shown in **Figure S6, 3**a-c, and **Table S2** are 2D GIWAXS pattern and related morphological parameters of pure PTFB-O, PTFB-O/ITIC-Th SqP, and PTFB-O:ITIC-Th BC films. For all the annealed samples, including both SqP and BC, the (010) coherence lengths (2.9-3.4 nm) and d-spacing (3.59 Å) are much the same, which shows that the polymer crystallinity of PTFB-O is maintained for SqP and BC annealed samples compared to the pure polymer. Both SqP and BC shows (100) lamellar stacking in in-plane as well as out-of-plane direction, and strong (010) π-π stacking peak is clearly observable in out-of-plane direction for all the cases indicating both SqP and BC prefers the face-on orientation that is beneficial for charge transport in the vertical direction (favorable direction for OPV application).[50] The high fill factor (FF) for all the conventional devices is consistent with the preferred face-on orientation. The hole and electron mobilities are measured using space charge limited current (SCLC) technique. The hole mobilities of SqP (7.7 x 10^{-4} cm^2 V^{-1} s^{-1}) is somewhat larger than the BC devices (5.3 x 10^{-4} cm^2 V^{-1} s^{-1}) owing to the slightly larger (010) coherence length of SqP (3.42 nm) compared to BC (3.36 nm). These results quite evidently demonstrate that the

TDA polymer's crystallinity can be well maintained and controlled by SqP method. Even the (010) coherence length of ITIC-Th is somewhat larger for SqP (3.25 nm) when compared to BC (3.05 nm) which shows the better molecular packing of ITIC-Th can be achieved using SqP method. The decent mobilities can be related to high FF (close to 75%) in both SqP and BC devices.

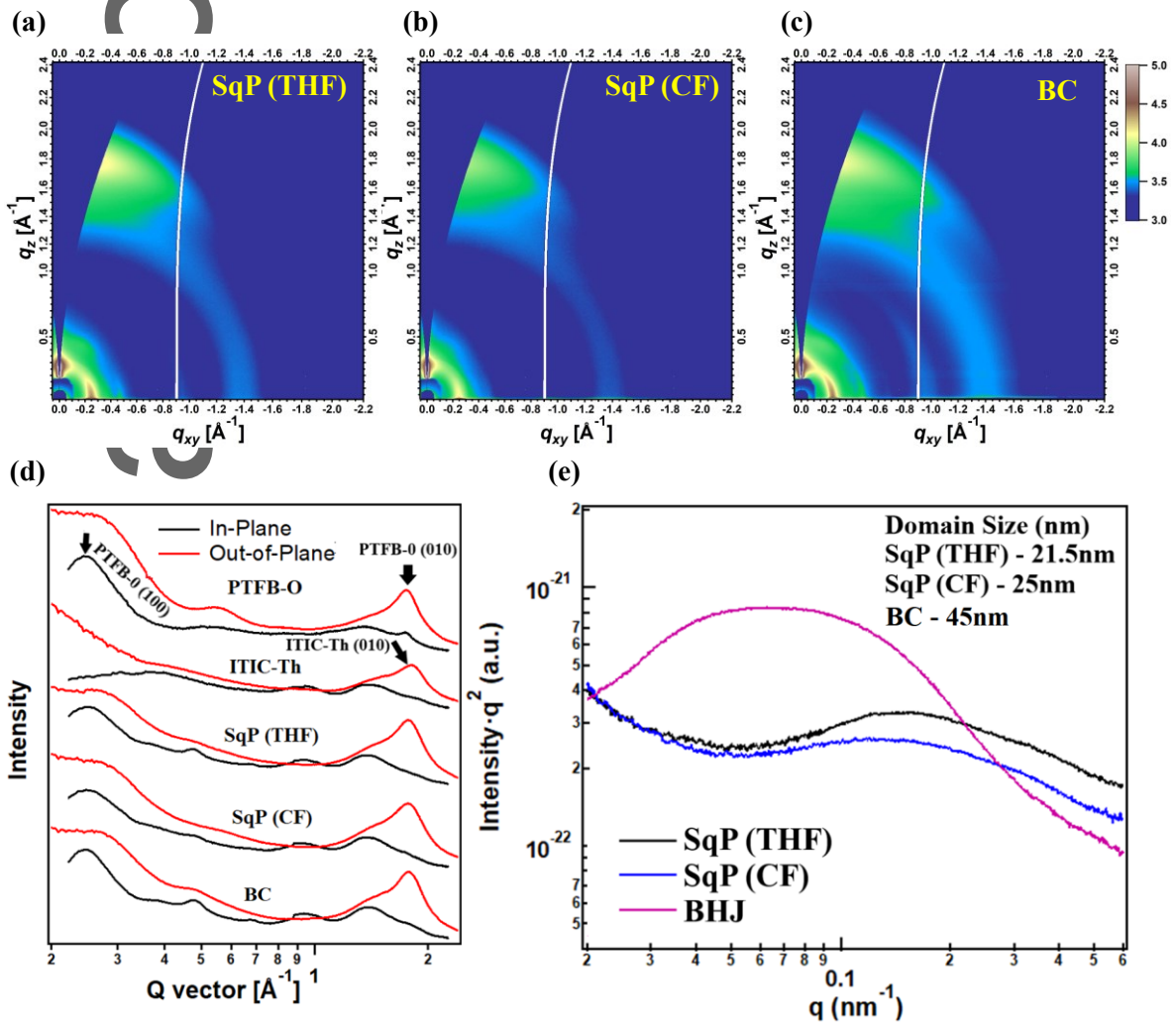

Figure 3. a-c) 2D GIWAXS patterns for PTFB-O/ITIC-Th, (a) SqP (THF), (b) SqP (CF), and (c) PTFB-O:ITIC-Th BC. d) 1D cuts of 2D GIWAXS patterns for pure PTFB-O, PTFB-O/ITIC-Th SqP, and PTFB-O:ITIC-Th BC films, and e) Normalized R-SoXS profiles for SqP and BC films (Inset: domain size).

The most dramatic difference between SqP and BC films is revealed by the R-SoXS data (**Figure 3**e **and Table S2**), which disclose the domain size and domain purity of the active layer film. The domain size of SqP films falls in the range of the most commonly accepted ideal domain size (20-30 nm) required for better performing OPV devices.[51] Whereas, a significantly larger domain size (45 nm) of the BC film explains the inferior performance when compared to SqP counterparts. This result matches well with the better PL quenching efficiency of SqP films discussed above. So, the higher J_{SC} in SqP devices can be explained by their optimum domain size which results in overall better performance. We note that the best performing SqP and BC devices show nearly the same V_{oc} and FF, which indicates that the charge recombination dynamics in these systems are similar despite the difference in domain sizes.[52] The critical point of morphological control is its ability to precisely achieve better polymer crystallinity with desirable domain size which helps to achieve better performing OPV devices.[40] Regarding the domain size variation between SqP and BC method, we hypothesize that in the case of BC method, the small molecule acceptor (SMA) might undergo excessive aggregation leading to larger domain size. This is quite evident from our previous work, where the addition of additives like 1,8-diiodooctane (DIO) or 1-chloronaphthalene (CN) yielded abysmal performance.[44] Whereas for SqP, we speculate that the extended drying process of TDA polymer film is beneficial for forming a favorable morphology before spin casting the acceptor layer. In this case, during the deposition of top acceptor layer, we suspect that the amorphous regions of polymer film might undergo swelling leading way for the acceptor to intercalate into the polymer film forming desired D/A morphology. In our case, it is quite apparent from our device performance and morphological characterizations how SqP method using TDA polymer can help in achieving desired morphology with better control and reproducibility.

Achieving desirable nano-scale morphology in small area devices (5.9 mm^2) inspired us to make devices with a larger area (50 mm^2), to get implication whether SqP method can achieve better performance during scale-up. The large area devices are made using the same processing conditions as small area devices. As shown in **Table 2**, even large area SqP devices can easily outdo the BC devices, showing real potential to transcend to printable OPVs.

Table 2. shows the photovoltaic performances of PTFB-O based large area devices

Device Area (mm^2)	Active Layer Combinations	V_{OC} [V]	J_{SC} [mA/cm^2]	FF	PCE [%]
50	SqP PTFB-O/ITIC-Th	0.93	17.21	0.63	10.12
	BC PTFB-O:ITIC-Th	0.94	13.75	0.64	8.31

2.3. DSIMS Analysis

The results of GIWAXS and RSoXS reveal the main reason for the higher PCE of SqP devices relative to the BC ones, but it could not fully explain the difference in device performance between inverted and conventional structures (e.g., why the SqP device performs better in conventional structure than in inverted structure). To explore the reasons behind it, we investigated the vertical phase segregation of the SqP and BC active layer films by carrying out DSIMS experiments by tracing the elements of individual materials along the entire film. Since only PTFB-O contains fluorine (F), we took advantage of this feature to

track the composition of F along the entire active layer film **(Figure 4)**. Even though the F content is slightly richer at the bottom surface for SqP deposition method (related to vertical phase segregation of PTFB-O), it is widely distributed all along the film. In other words, the SqP method does not create any 'bilayer-like' active layer where most acceptor stays on the top. Instead, SqP makes the acceptor and donor well distributed across the active layer, particularly in the middle region, e.g., from 20 nm to 80 nm considering a 100 nm – thick film (thickness of both films were controlled at ~100 nm), with only difference in the regions near the top and bottom interfaces, e.g., 0-20 nm and 80-100 nm. This again proves that the solvent of the acceptor enables the interdiffusion between donor and acceptor. More interestingly, both SqP and BC active layers show more polymer distributed in the lower part (toward the substrate) of the film while more acceptors are located near the top (airside) surface. Such vertical phase segregation explains why the conventional device structure outperforms the inverted one for both SqP and BC.

Furthermore, unlike the almost uniform distribution of fullerenes in SqP PffBT4T-2OD/$PC_{71}BM$ based annealed device (**Figure S3**), the comparison between SqP and BC for PTFB-O based devices reveals that SqP has more ITIC-Th near the top and more donor polymer near the bottom than the BC, evidenced by the higher F signal of the BC film at ~5-10 nm and sharper drop of F signal in the range of 80-100 nm of the BC film. This result, although it may not be the main reason, could also contribute to the difference in device performance between SqP and BC and is consistent with the trend in device parameters. Additionally, our data clearly shows that the polymer film is more influenced by swelling upon deposition of NFAs which is typically processed by high vapor pressure solvents like THF or CF. As reported by Aguirre et al. the amount of underlying polymer film swelling is determined by top acceptor's solvent as well as post-treatment like thermal annealing (TA) or

solvent vapor annealing (SVA).[34] In our case, even in the SqP as-cast film, the F distribution is almost identical to the ones with post-thermal treatment. These results prove that our processing conditions allow the TDA polymer to swell well and pave the way for interdiffusion of acceptors into the polymer film to establish an interpenetrating network which is reproducible as well as provides better control over the nano-scale morphology.

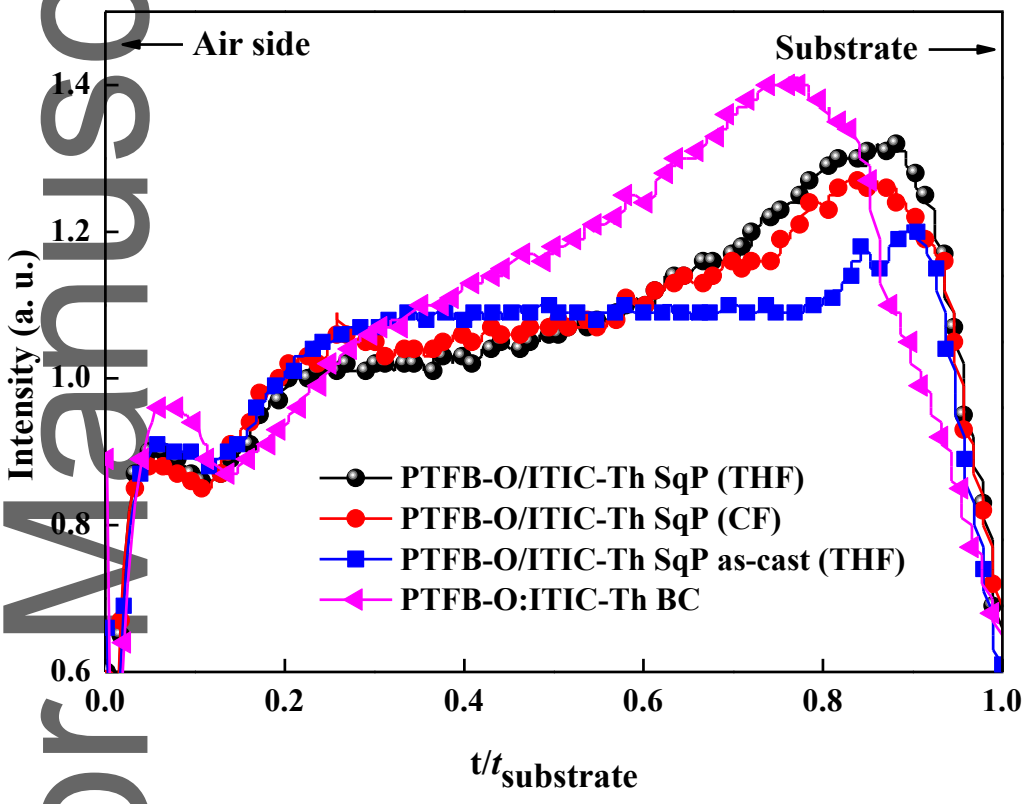

Figure 4. Fluorine (polymer) distribution of PTFB-O based SqP and BC processed active layer films measured using DSIMS.

2.4. Recombination Analysis

To further get the insight of device performance, we performed light intensity (*I*) studies to evaluate the charge recombination in both SqP and BC devices (**Figure 5** and **Table 1**). In OPVs, bimolecular and trap-assisted recombinations are the most dominant mechanisms for

the loss of photogenerated free charge carriers which will hurt the overall device performance.[53] Firstly, light intensity dependence of J_{SC} has been carried out by plotting them in logarithmic scale. It is widely accepted, under different illumination intensities, when the α in the power law dependence ($J_{SC} \propto I^{\alpha}$) is close to unity, it indicates the weak bimolecular recombination in the device.[54-55] In the case of SqP devices processed using THF for both conventional and inverted structures, α is close to unity (~0.99), which shows that a minimal amount of charge carriers are lost because of bimolecular recombination. Whereas, for other SqP and BC devices, slightly more bimolecular recombination (α = 0.96-0.97) is observed. To some extent, the variation in the J_{SC} of the devices can be attributed to the changes in the values of α.

Next, to assess the trap-assisted recombination in the device, we measured the V_{OC} of the SqP and BC devices under different light intensities, which allowed us to obtain the ideality factor n_{ideal} through $n_{ideal} = \frac{q\ \partial Voc}{kT\ \partial \ln(I)}$, where q is an elementary charge, k is the Boltzmann constant, T is the absolute temperature, and I is the light intensity.[56] Based on diodic theory, n_{ideal} should fall in the range of 1-2, and n_{ideal} values greater than unity indicates more trap-assisted recombination in the device.[56] We found that all SqP devices, including the ones with different solvents, along with the BC devices in the conventional structure, show small n_{ideal}s in the range of ~1.1-1.2, while the inverted BC device shows a n_{ideal} of >1.5, which is consistent to its inferior device performance, and could be related to more surface recombination[52] induced by the aforementioned undesired vertical phase segregation (Figure 5b and 4). Overall, the SqP samples demonstrate small bimolecular recombination and trap-assisted recombination, which corresponds well with their high FFs.

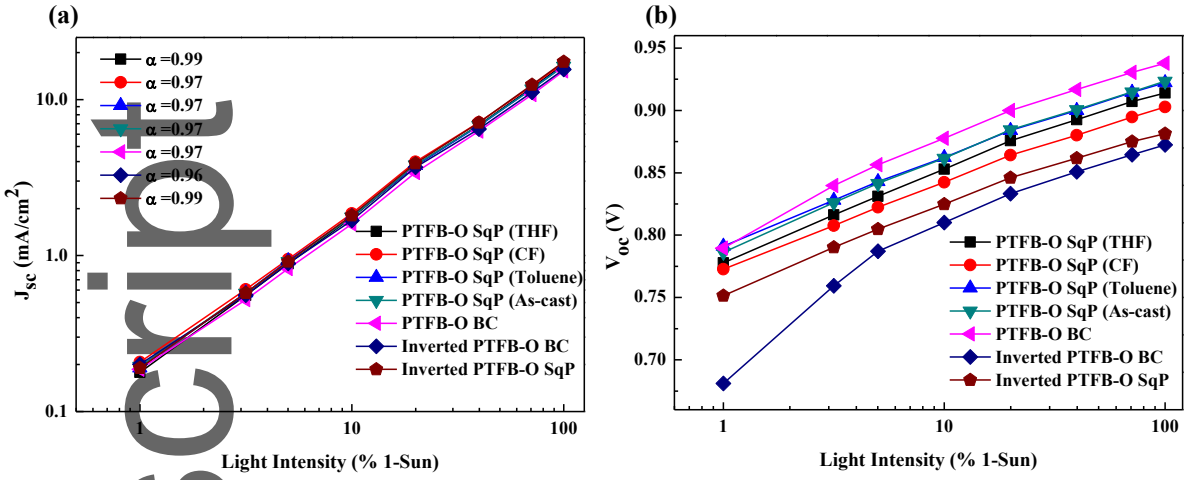

Figure 5. Recombination analysis. a) J_{SC} versus light intensity, and b) V_{OC} versus light intensity.

2.5. Sequential Processing Method using Five Different Solvents for the Acceptor

Furthermore, to support our claim of using many non-orthogonal solvents to process acceptors in sequential deposition method, we used another commonly used TDA material for non-fullerene OPVs named P3TEA.[57-59] For SqP based devices, P3TEA is dissolved in 1,2,4-trimethylbenzene (TMB), and the acceptor IT4F is processed using as many as five different solvents including CF, THF, toluene, CB, and o-Xylene, whose boiling points are 61.2 °C, 66 °C, 110.6 °C, 132 °C and 144.4 °C, respectively. For comparison, we fabricated BC based devices where the active layer is dissolved in TMB with the weight ratio of 1:1 (P3TEA:IT4F). As shown in **Table 3**, sequentially processed OPV devices outperformed the BC devices using all the different solvents. We believe, this is the first time that the SqP OPV device has been reported processing the top acceptor layer using various non-orthogonal solvents, wherein every single case can yield superior performance when compared to BC OPVs.

Table 3. Photovoltaic performances of P3TEA based devices

Active Layer Processing Method	Acceptor Processing Solvents	V_{OC} (V)	J_{SC} (mA/cm^2)	FF	PCE (%)
SqP P3TEA/IT4F	CF	0.83	16.00	0.71	9.48
	THF	0.82	17.32	0.69	9.80
	Toluene	0.83	16.15	0.70	9.38
	CB	0.84	15.42	0.74	9.55
	o-Xylene	0.83	15.40	0.75	9.58
BC P3TEA:IT4F	Co-dissolved in TMB	0.82	15.41	0.69	8.76

3. Conclusion

In summary, we fabricated OPV devices using sequential processing method with temperature-dependent aggregation donor polymers. We also showed how TDA polymer's insolubility at room temperature gives us feasibility to use a wide range of solvents during deposition of the top acceptor layer. Compared to their BC counterparts, SqP OPV devices showed superior performance owing to their better control in morphology as depicted by GIWAXS and R-SoXS data. The best and optimized PCE of SqP PTFB-O/ITIC-Th is 11.8% compared to their equivalent BC device which is 10.4%. The similar trend was followed even for SqP P3TEA/IT4F devices, which further supports our strategy by using as many as five different solvents that have largely different boiling points. Not only that, but we have also shown just by using the same active layer processing conditions but different device architecture, still SqP devices can easily outperform their corresponding BC devices. Additionally, we have analyzed the differences in performance using electrical and optical characterizations. Further, we went onto make devices with a larger area (50 mm^2) demonstrating the highest PCE of 10.12% (SqP device) which is ~18% higher than that of BC device. These results show the degree of freedom that TDA polymers possess which allows us to use various solvents including high boiling solvents which is critical in printing technologies. The flexibility to use various solvents, different device architecture with better control in morphology and higher PCE, SqP method using TDA polymers is highly promising for large scale production of OPV devices in the future.

4. Experimental section

4.1. OPV Device Fabrication

For all the OPV devices, prepatterned ITO-coated glass substrates (sheet resistance of 15 Ω/□) were cleaned using ultrasonic cleaner in detergent, deionized water, acetone, and isopropanol successively for 30 minutes each step. UV-ozone treatment using Novascan, PSD series digital ultraviolet ozone system was performed for 30 minutes before the substrates were transferred to a dry air-filled glovebox either to spin coat PEDOT:PSS or ZnO based on the device configurations.

4.1.1. Interlayer Processing Conditions: For conventional structure using ITO/PEDOT:PSS/active layer/PFN-Br/Ag, PEDOT:PSS (Al 4083) was spin-coated onto the ITO substrates at 5,000 rpm for 30 s and then annealed at 150 °C for 12 mins. PFN-Br was dissolved in methanol at the concentration of 0.5 mg/ml and spin coated at 2000 rpm for 30 s on the active layer film. Later, Ag (~250 nm) was thermally evaporated at a vacuum level of $\leq 1.5 \times 10^{-4}$ Pa at rates between 2-5 Å/s. For inverted structure using ITO/ZnO/active layer/MoO_3 + PEDOT:PSS (solution processable) or MoO_3 (thermally evaporated)/Ag, sol-gel zinc oxide (ZnO) was prepared by mixing 50 mg of zinc acetate dihydrate with 1 ml of 2-methoxy ethanol and 20 µl of ethanolamine and kept on stirring at room temperature for minimum of 10 hrs. Later, ZnO was spin coated on ITO substrates at 5000 rpm for 30 s followed by immediate annealing at 225 °C for 30 mins. For MoO_3 + PEDOT:PSS (solution processing), MoO_3 solution was prepared using the procedure mentioned[60] and mixed with PEDOT:PSS (Al 4083) to form a thin layer on active layer film. For evaporated MoO_3, samples were transferred into the thermal evaporator after spin coating the active layer film and subsequently depositing MoO_3 (~7 nm) and Ag (~250 nm) at rates below 1 Å/s once vacuum level reaches $\leq 1.5 \times 10^{-4}$ Pa.

4.1.2. PTFB-O based Active Layer Formation: For SqP method, PTFB-O (~50 nm) with the concentration of 10 mg/ml was dissolved in chlorobenzene (CB) by stirring at 100 °C for 2hrs, and spin coated at 2000 rpm for 1 min from a hot solution. ITIC-Th with the concentration of 10-25 mg/ml was dissolved either in tetrahydrofuran (THF) or chloroform (CF) or toluene for 2hrs at room temperature and spin coated instantaneously above PTFB-O layer at 2000-3000 rpm to form a thin layer of ~50 nm. For BC, PTFB-O:ITIC-Th (~100 nm) was dissolved in CB with the weight ratio of 1:1.5 with the donor concentration of 8 mg/ml and stirred at 100 °C for 2hrs before spin coating at 2000 rpm for 1 min. For both SqP and BC devices, the active layer film was annealed at 100 °C for 10 mins.

4.1.3. P3TEA based Active Layer Formation: For SqP method, P3TEA with the concentration of 12 mg/ml was dissolved in 1,2,4-trimethylbenzene (TMB) by stirring at 100 °C for 2hrs, and spin coated at 2000 rpm for 1 min from a hot solution. IT4F with the concentration of 10-25 mg/ml was dissolved either in THF, CF, toluene, o-xylene, and CB for 2hrs at room temperature and spin coated instantaneously above P3TEA layer at 2000-3000 rpm to form a thin film. For BC, P3TEA:IT4F was dissolved in TMB with the weight ratio of 1:1 with the donor concentration of 9 mg/ml and stirred at 100 °C for 2hrs before spin coating at 2000 rpm for 1min. For both SqP and BC devices, the active layer film was annealed at 100 °C for 10 mins.

4.2. Measurements and Instruments

After electrode deposition, the devices were encapsulated using EPO-TEK (OG154-1) epoxy in the nitrogen-filled glove box and transferred to ambient conditions to further conduct *J–V* measurements using a Keithley 2400 source meter unit under AM 1.5G (100 mW/cm^2) by a Newport solar simulator. The light intensity was calibrated using a standard Si diode (with

KG5 filter, purchased from PV Measurement) to bring spectral mismatch to unity. For light intensity dependent *J–V* measurements, a series of neutral color density filters were employed to vary the light intensity from 1-sun to 1% 1-sun. Typical cells have a device area of either 5.9 mm^2 or 50 mm^2, defined by a metal mask with an aperture aligned with the device area. The photovoltaic performance of the devices was not confirmed from independent certification laboratories. External quantum efficiency (EQE) spectra were measured using an EQE (Enlitech QS) system equipped with a standard Si diode with the monochromatic light generated from a Newport 300 W lamp source.

4.3. GIWAXS and RSoXS

4.3.1. GIWAXS Characterization: GIWAXS measurements were performed at beamline 7.3.3[61] at the Advanced Light Source (ALS). Samples were prepared on Si substrates using same blend solutions like those used in devices. 10 keV X-ray beam was incident at a grazing angle of 0.12-0.15°, which maximized the scattering intensity from the samples. The scattered X-rays were detected using a Dectris Pilatus 1-M photon counting detector. Samples were prepared on Si substrates. All measurements were conducted under a helium atmosphere to reduce air scattering.

4.3.2. R-SoXS Characterization: R-SoXS transmission measurements were performed at beamline 11.0.1.2[62] at the ALS. Samples for R-SoXS measurements were prepared on a PSS modified Si substrate under the same conditions as those used for device fabrication, and then transferred by floating in water to a 1.5×1.5 mm, 100 nm thick Si_3N_4 membrane supported by a 5×5 mm, 200 mm thick Si frame (Norcada Inc.). Two- dimensional scattering patterns were

collected on an in-vacuum CCD camera. The composition variation (related to the relative domain purity) over the length scales probed can be extracted by integrating scattering profiles to yield the integrated scattering intensity (ISI). The purer the average domains are, the higher the ISI. Owing to a lack of absolute flux normalization, the absolute composition cannot be obtained by only R-SoXS.

4.4. Dynamic SIMS

Dynamic SIMS experiment was conducted using a TOF SIMS V (ION-TOF GmbH, Cameca IMS 4f). Bi_3^+ (25 keV) was used as the primary ion and Cs^+ (3 keV) was utilized as the sputtering source. The area of analysis was in the range of (54 × 54) – (61 × 61) μm^2 and while the sputtering area was 300 × 300 μm^2.

Supporting Information

Supporting Information is available from the Wiley Online Library or the author.

Acknowledgments

L. Arunagiri, G. Zhang, and H. Hu contributed equally to this work. The work described in this paper was partially supported by the National Basic Research Program of China (973 Program project numbers 2013CB834701 and 2014CB643501), the Hong Kong Research Grants Council (project numbers T23–407/13 N, N_HKUST623/13, 16305915, 16322416 and 606012), HK JEBN Limited, HKUST president's office (Project FP201) and the National Science Foundation of China (#21374090). We especially thank the Hong Kong Innovation and Technology Commission for the support through projects ITC-CNERC14SC01 and ITS/083/15. X-ray data were acquired at beamlines 11.0.1.2 and 7.3.3 at the Advanced Light Source, which is supported by the Director, Office of Science, Office of Basic Energy Sciences, of the U.S. Department of Energy under Contract No. DE-AC02-05CH11231.

Received: ((will be filled in by the editorial staff))
Revised: ((will be filled in by the editorial staff))
Published online: ((will be filled in by the editorial staff))

References

[1] J. Liu, S. Chen, D. Qian, B. Gautam, G. Yang, J. Zhao, J. Bergqvist, F. Zhang, W. Ma, H. Ade, *Nat. Energy* **2016**, *1*, *16089*.

[2] H. Bin, L. Gao, Z.-G. Zhang, Y. Yang, Y. Zhang, C. Zhang, S. Chen, L. Xue, C. Yang, M. Xiao, *Nat. Commun.* **2016**, *7*, *13651*.

[3] D. Baran, R. S. Ashraf, D. A. Hanifi, M. Abdelsamie, N. Gasparini, J. A. Röhr, S. Holliday, A. Wadsworth, S. Lockett, M. Neophytou, *Nat. Mater.* **2017**, *16*, *363*.

[4] Y. Gao, D. Li, Z. Xiao, X. Qian, J. Yang, F. Liu, S. Yang, L. Ding, *Mater. Chem. Front.* **2019**, *3*, *399*.

[5] X. Zhan, S. R. Marder, *Mater. Chem. Front.* **2019**, *3*, *180*.

[6] X. Shi, X. Liao, K. Gao, L. Zuo, J. Chen, J. Zhao, F. Liu, Y. Chen, A. K. Y. Jen, *Adv. Funct. Mater.* **2018**, *28*, *1802324*.

[7] C. Yan, S. Barlow, Z. Wang, H. Yan, A. K.-Y. Jen, S. R. Marder, X. Zhan, *Nat. Rev. Mater.* **2018**, *3*, *18003*.

[8] Y. Fang, A. K. Pandey, D. M. Lyons, P. E. Shaw, S. E. Watkins, P. L. Burn, S. C. Lo, P. Meredith, *ChemPhysChem.* **2015**, *16*, *1295*.

[9] J. Yuan, T. Huang, P. Cheng, Y. Zou, H. Zhang, J. L. Yang, S.-Y. Chang, Z. Zhang, W. Huang, R. Wang, *Nat. Commun.* **2019**, *10*, *570*.

[10] H. Cha, J. Wu, A. Wadsworth, J. Nagitta, S. Limbu, S. Pont, Z. Li, J. Searle, M. F. Wyatt, D. Baran, *Adv. Mater.* **2017**, *29*, *1701156*.

[11] Y.-Q.-Q. Yi, H. Feng, N. Zheng, X. Ke, B. Kan, M. Chang, Z. Xie, X. Wan, C. Li, Y. Chen, *Chem. Mater.* **2019**, *31*, *904*.

[12] J. Yu, P. Chen, C. W. Koh, H. Wang, K. Yang, X. Zhou, B. Liu, Q. Liao, J. Chen, H. Sun, *Adv. Sci.* **2019**, *6*, *1801743*.

[13] P. Cheng, J. Wang, Q. Zhang, W. Huang, J. Zhu, R. Wang, S. Y. Chang, P. Sun, L. Meng, H. Zhao, *Adv. Mater.* **2018**, *30*, *1801501*.

[14] P. Cheng, Y. Liu, S.-Y. Chang, T. Li, P. Sun, R. Wang, H.-W. Cheng, T. Huang, L. Meng, S. Nuryyeva, *Joule* **2019**, *3*, *432*.

[15] J. Zhang, L. Zhu, Z. Wei, *Small Methods* **2017**, *1*, *1700258*.

[16] S. Zhang, Y. Qin, J. Zhu, J. Hou, *Adv. Mater.* **2018**, *30*, *1800868*.

[17] Y. Zhang, B. Kan, Y. Sun, Y. Wang, R. Xia, X. Ke, Y. Q. Q. Yi, C. Li, H. L. Yip, X. Wan, *Adv. Mater.* **2018**, *30*, *1707508*.

[18] J. Yuan, Y. Zhang, L. Zhou, G. Zhang, H.-L. Yip, T.-K. Lau, X. Lu, C. Zhu, H. Peng, P. A. Johnson, *Joule* **2019**, *3*, *908*.

[19] L. Meng, Y. Zhang, X. Wan, C. Li, X. Zhang, Y. Wang, X. Ke, Z. Xiao, L. Ding, R. Xia, *Science* **2018**, *361*, *1094*.

[20] R. Søndergaard, M. Hösel, D. Angmo, T. T. Larsen-Olsen, F. C. Krebs, *Mater. Today.* **2012**, *15*, *36*.

[21] H. W. Ro, J. M. Downing, S. Engmann, A. A. Herzing, D. M. DeLongchamp, L. J. Richter, S. Mukherjee, H. Ade, M. Abdelsamie, L. K. Jagadamma, *Energy Environ. Sci.* **2016**, *9*, *2835*.

[22] P. W. Blom, V. D. Mihailetchi, L. J. A. Koster, D. E. Markov, *Adv. Mater.* **2007**, *19*, *1551*.

[23] X. Guo, M. Zhang, J. Tan, S. Zhang, L. Huo, W. Hu, Y. Li, J. Hou, *Adv. Mater.* **2012**, *24*, *6536*.

[24] A. Mayer, M. F. Toney, S. R. Scully, J. Rivnay, C. J. Brabec, M. Scharber, M. Koppe, M. Heeney, I. McCulloch, M. D. McGehee, *Adv. Funct. Mater.* **2009**, *19*, *1173*.

[25] J. Zhao, Y. Li, G. Yang, K. Jiang, H. Lin, H. Ade, W. Ma, H. Yan, *Nat. Energy* **2016**, *1*, *15027*.

[26] C. McDowell, M. Abdelsamie, M. F. Toney, G. C. Bazan, *Adv. Mater.* **2018**, *30*, *1707114*.

[27] A. Armin, M. Hambsch, I. K. Kim, P. L. Burn, P. Meredith, E. B. Namdas, *Laser Photonics Rev.* **2014**, *8*, *924*.

[28] K. Zhang, Z. Chen, A. Armin, S. Dong, R. Xia, H. L. Yip, S. Shoaee, F. Huang, Y. Cao, *Sol. RRL* **2018**, *2*, *1700169*.

[29] F. C. Krebs, *Sol. Energy Mater Sol. Cells* **2009**, *93*, *394*.

[30] A. L. Ayzner, C. J. Tassone, S. H. Tolbert, B. J. Schwartz, *J. Phys. Chem. C* **2009**, *113*, *20050*.

[31] D. H. Wang, H. K. Lee, D.-G. Choi, J. H. Park, O. O. Park, *Appl. Phys. Lett.* **2009**, *95*, *043505*.

[32] S. A. Hawks, J. C. Aguirre, L. T. Schelhas, R. J. Thompson, R. C. Huber, A. S. Ferreira, G. Zhang, A. A. Herzing, S. H. Tolbert, B. J. Schwartz, *J. Phys. Chem. C* **2014**, *118*, *17413*.

[33] G. Zhang, R. C. Huber, A. S. Ferreira, S. D. Boyd, C. K. Luscombe, S. H. Tolbert, B. J. Schwartz, *J. Phys. Chem. C* **2014**, *118*, *18424*.

[34] J. C. Aguirre, S. A. Hawks, A. S. Ferreira, P. Yee, S. Subramaniyan, S. A. Jenekhe, S. H. Tolbert, B. J. Schwartz, *Adv. Energy Mater.* **2015**, *5*, *1402020*.

[35] P. Cheng, R. Wang, J. Zhu, W. Huang, S. Y. Chang, L. Meng, P. Sun, H. W. Cheng, M. Qin, C. Zhu, *Adv. Mater.* **2018**, *30*, *1705243*.

[36] Y. Cui, S. Zhang, N. Liang, J. Kong, C. Yang, H. Yao, L. Ma, J. Hou, *Adv. Mater.* **2018**, *30*, *1802499*.

[37] S. Dong, K. Zhang, B. Xie, J. Xiao, H. L. Yip, H. Yan, F. Huang, Y. Cao, *Adv. Energy Mater.* **2018**, *9*, *1802832*.

[38] J. Zhang, B. Kan, A. J. Pearson, A. J. Parnell, J. F. Cooper, X.-K. Liu, P. J. Conaghan, T. R. Hopper, Y. Wu, X. Wan, *J. Mater. Chem. A* **2018**, *6*, *18225*.

[39] J. Min, R. Sun, J. Guo, C. Sun, Z. Luo, Z. Zhang, X. Jiao, W. Tang, C. Yang, Y. Li, *Energy Environ. Sci.* **2019**, *12*, *384*.

[40] H. Hu, P. C. Chow, G. Zhang, T. Ma, J. Liu, G. Yang, H. Yan, *Acc. Chem. Res.* **2017**, *50*, *2519*.

[41] K. Jiang, G. Zhang, G. Yang, J. Zhang, Z. Li, T. Ma, H. Hu, W. Ma, H. Ade, H. Yan, *Adv. Energy Mater.* **2018**, *8*, *1701370*.

[42] H. Yao, Y. Li, H. Hu, P. C. Chow, S. Chen, J. Zhao, Z. Li, J. H. Carpenter, J. Y. L. Lai, G. Yang, *Adv. Energy Mater.* **2018**, *8*, *1701895*.

[43] Y. Liu, J. Zhao, Z. Li, C. Mu, W. Ma, H. Hu, K. Jiang, H. Lin, H. Ade, H. Yan, *Nat. Commun.* **2014**, *5*, *5293*.

[44] Z. Li, K. Jiang, G. Yang, J. Y. L. Lai, T. Ma, J. Zhao, W. Ma, H. Yan, *Nat. Commun.* **2016**, *7*, *13094*.

[45] Y. Lin, F. Zhao, Q. He, L. Huo, Y. Wu, T. C. Parker, W. Ma, Y. Sun, C. Wang, D. Zhu, *J. Am. Chem. Soc.* **2016**, *138*, *4955*.

[46] W. Zhao, S. Li, H. Yao, S. Zhang, Y. Zhang, B. Yang, J. Hou, *J. Am. Chem. Soc.* **2017**, *139*, *7148*.

[47] S. A. Mauger, L. Chang, S. Friedrich, C. W. Rochester, D. M. Huang, P. Wang, A. J. Moulé, *Adv. Funct. Mater.* **2013**, *23*, *1935*.

[48] S. Rait, S. Kashyap, P. Bhatnagar, P. Mathur, S. Sengupta, J. Kumar, *Sol. Energy Mater Sol. Cells* **2007**, *91*, *757*.

[49] N. S. Sariciftci, L. Smilowitz, A. J. Heeger, F. Wudl, *Science* **1992**, *258*, *1474*.

[50] V. Vohra, K. Kawashima, T. Kakara, T. Koganezawa, I. Osaka, K. Takimiya, H. Murata, *Nat. Photonics* **2015**, *9*, *403*.

[51] A. J. Heeger, *Adv. Mater.* **2014**, *26*, *10*.

[52] G. Zhang, J. Zhao, P. C. Chow, K. Jiang, J. Zhang, Z. Zhu, J. Zhang, F. Huang, H. Yan, *Chem. Rev.* **2018**, *118*, *3447*.

[53] C. Brabec, U. Scherf, V. Dyakonov, *Organic photovoltaics: materials, device physics, and manufacturing technologies*, John Wiley & Sons, **2011**.

[54] L. Koster, V. Mihailetchi, H. Xie, P. Blom, *Appl. Phys. Lett.* **2005**, *87*, *203502*.

[55] Z. Li, J. D. Lin, H. Phan, A. Sharenko, C. M. Proctor, P. Zalar, Z. Chen, A. Facchetti, T. Q. Nguyen, *Adv. Funct. Mater.* **2014**, *24*, *6989*.

[56] G. Wetzelaer, M. Kuik, M. Lenes, P. Blom, *Appl. Phys. Lett.* **2011**, *99*, *153506*.

[57] A. D. Hendsbee, J.-P. Sun, W. K. Law, H. Yan, I. G. Hill, D. M. Spasyuk, G. C. Welch, *Chem. Mater.* **2016**, *28*, *7098*.

[58] P. Cheng, G. Li, X. Zhan, Y. Yang, *Nat. Photonics* **2018**, *12*, *131*.

[59] J. Zhang, Y. Li, J. Huang, H. Hu, G. Zhang, T. Ma, P. C. Chow, H. Ade, D. Pan, H. Yan, *J. Am. Chem. Soc.* **2017**, *139*, *16092*.

[60] F. Xie, W. C. Choy, C. Wang, X. Li, S. Zhang, J. Hou, *Adv. Mater.* **2013**, *25*, *2051*.

[61] A. Hexemer, W. Bras, J. Glossinger, E. Schaible, E. Gann, R. Kirian, A. MacDowell, M. Church, B. Rude, H. Padmore, "A SAXS/WAXS/GISAXS beamline with multilayer monochromator", presented at XIV International Conference on Small-Angle Scattering (SAS09), Oxford, UK, **2010**.

[62] E. Gann, A. Young, B. Collins, H. Yan, J. Nasiatka, H. Padmore, H. Ade, A. Hexemer, C. Wang, *Rev. Sci. Instrum.* **2012**, *83*, *045110*.

The table of contents entry

Sequentially processed organic photovoltaics (SqP OPVs) using temperature-dependent aggregation (TDA) polymers where the acceptor materials have been processed using various non-orthogonal solvents providing almost similar performance in every single case. The superior performance when compared to their BC counterparts can be attributed to better control in morphology which is critical for large-area scale-up of OPVs.

Keywords: organic photovoltaic, sequential processing method, bulk heterojunction, non-orthogonal solvents, temperature-dependent aggregation

Lingeswaran Arunagiri, Guangye Zhang,* Huawei Hu, Huatong Yao, Kai Zhang, Yunke Li, Philip C. Y. Chow, Harald Ade, and He Yan*

Temperature-Dependent Aggregation Donor Polymers Enables Highly Efficient Sequentially Processed Organic Photovoltaics without the Need of Orthogonal Solvents